ELSEVIER

Journal of Nuclear Materials 251 (1997) 89–97

journal of nuclear materials

Disorder-induced amorphization

Nghi Q. Lam *, Paul R. Okamoto, Mo Li [1]

Materials Science Division, Argonne National Laboratory, Argonne, IL 60439, USA

Abstract

Many crystalline materials undergo a crystalline-to-amorphous (c–a) phase transition when subjected to energetic particle irradiation at low temperatures. By focusing on the mean-square static atomic displacement as a generic measure of chemical and topological disorder, we are led quite naturally to a generalized version of the Lindemann melting criterion as a conceptual framework for a unified thermodynamic approach to solid-state amorphizing transformations. In its simplest form, the generalized Lindemann criterion assumes that the sum of the static and dynamic mean-square atomic displacements is constant along the polymorphous melting curve, so that c–a transformations can be understood simply as melting of critically-disordered crystals at temperatures below the glass transition temperature where the supercooled liquid can persist indefinitely in a configurationally-frozen state. Evidence in support of the generalized Lindemann melting criterion for amorphization is provided by a large variety of experimental observations and by molecular dynamics simulations of heat-induced melting and defect-induced amorphization of intermetallic compounds. © 1997 Elsevier Science B.V.

1. Introduction

Melting of a crystalline solid to a liquid is the most common and probably one of the most extensively studied phase transformations. Another phase transformation that produces a non-crystalline final state is solid-state amorphization. While the common link between the liquid and amorphous phases as non-crystalline states has long been recognized, the many similarities in the processes of heat-induced melting and solid-state amorphization have only recently been recognized [1–3]. Fundamental studies of radiation-driven crystalline-to-amorphous (c–a) transformations, which occur during ion implantation, ion-beam mixing, and, particularly, electron-, and ion-irradiation of intermetallic compounds [4–7], have led to a deeper understanding of the connection between c–a transition and melting. Early irradiation experiments on the ordered compound Zr_3Al revealed a number of thermodynamic parallels between these two disordering processes [2,3,6]. Of particular significance was the discovery that the gradual destruction of chemical long-range order precedes the onset of amorphization and that the disordering is accompanied by a large (~ 50%) decrease in the average shear modulus. This decrease is comparable in magnitude to the isobaric shear elastic softening associated with the heating to melting of many crystalline materials [8,9]. Subsequent investigations on other intermetallic compounds showed that the large disorder-induced softening is a characteristic precursor effect of c–a transformations [6,10–14]. Indeed, the melting temperatures of materials generally scale with the shear elastic constants [15] so that one can expect the melting temperature of a crystal to decrease with increasing amount of static atomic disorder. It is the purpose of the present paper to focus on this connection between atomic displacements and elastic softening which underlies many of the thermodynamic parallels between heat-induced melting and defect-induced amorphization.

2. Disorder-induced melting of metastable crystals

2.1. Generalization of the Lindemann melting criterion

By focusing on the static and dynamic components of the total mean-square atomic displacement as a generic measure of crystalline disorder, we are led quite naturally to a generalized version [16] of the Lindemann melting

* Corresponding author. Tel.: +1-630 252 4953; fax: +1-630 252 4798; e-mail: nghi_lam@qmgate.anl.gov.

[1] On leave from the Department of Applied Physics, California Institute of Technology, Pasadena, CA 91125, USA.

PII S0022-3115(97)00257-2

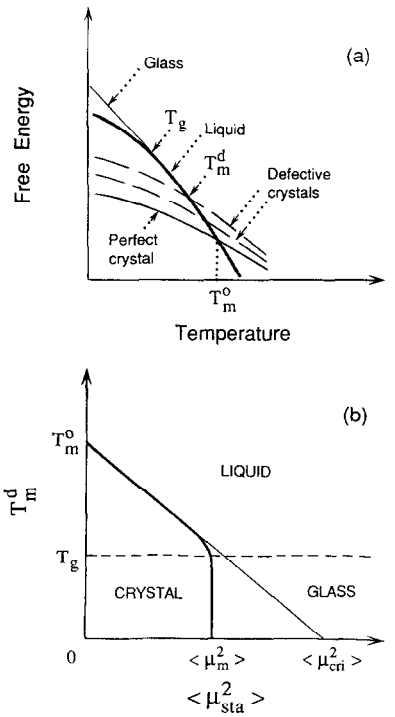

Fig. 1. Plots of (a) free energy versus temperature for the perfect crystal, liquid, glassy phase and various defective crystals, and (b) dependence of the melting temperature T_m^d on mean-square static atomic displacement $\langle \mu_{sta}^2 \rangle$, based on the generalized Lindemann melting criterion (thin straight line, Eqs. (3) and (4)) and on the thermodynamic criterion for amorphization (thick curve, Eqs. (3) and (7)). Here, $\langle \mu_m^2 \rangle$ and $\langle \mu_{cri}^2 \rangle$ denote the critical values of $\langle \mu_{sta}^2 \rangle$ for *thermodynamic* and *mechanical* melting.

criterion [17] as a conceptual basis for a unified thermodynamic description of heat-induced melting and disorder-induced amorphization [6,18–22]. The dynamic component, $\langle \mu_{vib}^2 \rangle$, scales directly with temperature and is a measure of the free energy associated with atomic vibrations. On the other hand, the static component, $\langle \mu_{sta}^2 \rangle$, is a measure of the static atomic disorder stored in the lattice in the form of intrinsic and extrinsic lattice defects which give rise to an increase in the free energy and, hence, to a decrease in the melting temperature, T_m^d, of the defective crystal. This effect is illustrated schematically in Fig. 1a where the Gibbs free energy as a function of temperature is shown for the glassy phase, the liquid phase and the perfect crystalline phase. Also shown are T_m^0, the thermodynamic melting temperature of the defect-free crystal, the glass transition temperature T_g at which the supercooled liquid freezes to a glass, and several metastable defective crystalline states representing different levels of static disorder as measured by $\langle \mu_{sta}^2 \rangle$. The melting curve of the defective crystalline state, defined by the locus of points $(T_m^d, \langle \mu_{sta}^2 \rangle)$ where the free energy curves of all possible metastable states intersect that of the liquid, is shown schematically in Fig. 1b. Reflecting the behavior of high-temperature region of the liquid free energy curve, T_m^d decreases approximately linearly with $\langle \mu_{sta}^2 \rangle$ up to a critical damage level $\langle \mu_m^2 \rangle$, where $T_m^d = T_g$. Beyond this point, T_m^d decreases sharply to zero, reflecting the non-linear behavior of the liquid free energy curve for $T \leq T_g$. All damage states on the right-hand side of the melting curve are liquid states if $T > T_g$, or amorphous states if $T \leq T_g$.

The linear region of the melting curve in Fig. 1b is in fact a graphical statement of the generalized Lindemann melting criterion which, in its simplest form [21,22], assumes that the sum $\langle \mu_{sta}^2 \rangle + \langle \mu_{vib}^2 \rangle$ remains constant along the melting curve. This condition can be expressed formally by

$$\langle \mu_{sta}^2 \rangle + \langle \mu_{vib}^2 \rangle = \langle \mu_{cri}^2 \rangle, \tag{1}$$

where, by hypothesis, $\langle \mu_{cri}^2 \rangle$ is a constant and, hence, must be equal to its value at the thermodynamic melting temperature, T_m^0, of the defect-free crystal. For a Debye solid, $\langle \mu_{vib}^2 \rangle$ in Eq. (1) is given by [23,24]

$$\langle \mu_{vib}^2 \rangle = \frac{9\hbar^2 T}{Mk\theta_0^2}, \tag{2}$$

where $\hbar$ is Plank's constant, M is the average atomic mass, k is the Boltzmann constant and θ_0 is the Debye temperature of the defect-free crystal. Hence, along the melting curve where $T = T_m^d$, Eq. (1) becomes

$$T_m^d = \frac{Mk\theta_d^2}{9\hbar^2} \langle \mu_{cri}^2 \rangle, \tag{3}$$

where θ_d, the effective Debye temperature for the defective crystal, is defined by

$$\theta_d^2 = \theta_0^2 \left[1 - \frac{\langle \mu_{sta}^2 \rangle}{\langle \mu_{cri}^2 \rangle} \right]. \tag{4}$$

For the defect-free crystal: $\langle \mu_{sta}^2 \rangle \to 0$, $\theta_d^2 \to \theta_0^2$ and $T_m^d \to T_m^0 \equiv (Mk\theta_0^2/9\hbar^2)\langle \mu_{cri}^2 \rangle$. Hence, Eq. (3) indicates that the linear behavior of the melting curve, shown schematically in Fig. 1b, follows directly from Eq. (4). Since θ_d^2 is directly proportional to the average shear modulus G_d [24], the decrease in melting temperature described by Eq. (3) should be directly observable as a disorder-induced softening of the average shear modulus of the same form as Eq. (4). Hence, a direct corollary of the generalized Lindemann melting criterion is that reduced quantities T_m^d/T_m^0, θ_d^2/θ_0^2 and G_d/G_0 all must be equal and have the same functional form, i.e.

$$\frac{T_m^d}{T_m^0} = \frac{\theta_d^2}{\theta_0^2} = \frac{G_d}{G_0} = \left[1 - \frac{\langle \mu_{sta}^2 \rangle}{\langle \mu_{cri}^2 \rangle} \right]. \tag{5}$$

The disorder-induced softening described by Eq. (5) is identical in form to the high-temperature softening associated with the isobaric heating of the defect-free crystal. This follows from Eq. (2) and from the temperature depen-

dence of the isobaric elastic constants of many metals, which is of the general form [23,24]

$$\frac{G_0(T)}{G_0(0)} \approx \exp(-T/T_{cri}). \tag{6}$$

Here, $G_0(0)$ is the average shear modulus at $T = 0$ K and T_{cri} is the temperature at which $G_0(T)$ extrapolates to zero on the temperature axis. Typically, $T_{cri} \gg T_m^0$ so that for $T \leq T_m^0$, Eq. (6) reduces to $G_0(T) = G_0(0)[1 - T/T_{cri}]$, which is identical in form to Eq. (5), since from Eq. (2), $T/T_{cri} = \langle \mu_{vib}^2 \rangle / \langle \mu_{cri}^2 \rangle$. Hence, within the framework of the generalized Lindemann melting criterion, the effect of static atomic disorder on the average shear modulus at constant temperature is identical to that of increasing temperature at constant pressure. Consequently, a single curve should be obtained for both isothermal disordering and isobaric heating when G_d/G_0 is plotted as a function of the total mean-square displacement, $\langle \mu_{tot}^2 \rangle = \langle \mu_{sta}^2 \rangle + \langle \mu_{vib}^2 \rangle$. It is interesting to note that this equivalence in the effects of heating and static atomic disorder on elastic properties reflects, to first order, their equivalent effects on the intensity of Bragg peaks in X-ray and electron diffraction patterns [25].

The real significance of this new conceptual approach to defect-induced amorphization is that it depends on the magnitude of $\langle \mu_{sta}^2 \rangle$, but not on how the static atomic displacements are produced. Hence, $\langle \mu_{sta}^2 \rangle$ can be a measure of the concentration of misfitting solute atoms in an alloy, the concentration of Frenkel pairs or antisite defects in irradiated materials, the dislocation density in deformed materials, and even the stress level in strained crystals. In the case of antisite defects in ordered binary compounds, $\langle \mu_{sta}^2 \rangle$ is a linear function of the mean-square chemical disorder defined by $(1 - \eta^2)$, where η is the Bragg–Williams long-range order parameter [26]. Moreover, the concept of disorder-induced melting is not limited to homogeneous defect structures but is applicable to heterogeneous defect structures such as local regions around impurity atoms [27], grain boundaries [28], and nanocrystals where $\langle \mu_{sta}^2 \rangle$ is a direct measure of inverse grain size [29], as well as to highly-strained crack tip regions of crystal where $\langle \mu_{sta}^2 \rangle$ provides a measure of stress level [30].

2.2. Thermodynamic and kinetic aspects of amorphization

As shown schematically by Fig. 1a and b, the generalized Lindemann melting criterion implies that it is thermodynamically possible for a sufficiently disordered crystal to undergo a disorder-induced melting process at any temperature below the thermodynamic melting temperature T_m^0 of the perfect crystal. In practice, however, disorder-induced melting will only be observable at temperatures below the glass transition temperature T_g where diffusional-relaxation processes in both the crystalline and amorphous phases are sufficiently slow to allow the buildup of the critical damage level required to drive the c–a transformation and, once formed, to prevent recrystallization of the amorphous phase. This kinetic constraint, $T_m^d \leq T_g$, is consistent with the thermodynamic criterion for amorphization since a thermodynamic driving force exits only for metastable crystalline states that have free energies equal to or higher than that of the amorphous phase. As illustrated in Fig. 1a, this is equivalent to the condition $T_m^d \leq T_g$. Under this condition, the free energy difference $\Delta F = \Delta H - T\Delta S$ between the crystalline and amorphous phases is due almost entirely to the difference in their enthalpies, ΔH, and the thermodynamic criterion for amorphization can be written formally as [22]

$$\frac{\Delta H_d}{\Delta H_g} = \frac{L_0 - L_d}{L_0 - L_g} = \left[\frac{\theta_0^2 - \theta_d^2}{\theta_0^2 - \theta_g^2}\right] \geq 1, \tag{7}$$

where ΔH_d and ΔH_g are, respectively, the enthalpies of the defective crystal and amorphous phase relative to that of the perfect crystal and L_0, L_d and L_g are the heats of fusion of the perfect crystal, defective crystal and amorphous phase. The equality in Eq. (7) derives from the fact that the heat of fusion scales in direct proportion to the melting temperature and, hence, to the square of the Debye temperature via the Lindemann scaling relationships defined by Eq. (5). Therefore, the inequality in Eq. (7) reduces to $\theta_d \leq \theta_g$ or, equivalently, to $G_d \leq G_g$ or $T_m^d \leq T_g$. All three inequalities are physically equivalent to the thermodynamic criterion for amorphization given by Eq. (7) and can be called 'Lindemann' criteria for amorphization since all three depend on the validity of the generalized Lindemann melting criterion expressed in the form of Eq. (5). The two elastic softening criteria for amorphization, $\theta_d \leq \theta_g$ and $G_d \leq G_g$, both of which have been verified experimentally [2,6,10–14] and by molecular dynamics simulations [22], are of considerable practical importance. In fact, the effect of static atomic disorder on the average shear moduli of crystalline and amorphous phases can be readily measured at very low temperatures, whereas the effect of static disorder on the melting temperatures, T_m^d, may not be directly measurable in materials where rapid damage annealing can occur during heating to T_m^d, particularly for low damage levels where $T_m^d \gg T_g$.

3. Confirmations of the generalized Lindemann melting criterion

3.1. Results of molecular dynamics simulations

Molecular dynamics simulations of radiation-induced amorphization in ordered intermetallic compounds have provided considerable insight into the atomic-scale mechanisms of c–a transformations. Early studies focused on: (i) the thermodynamic response of ordered compounds to the introduction of antisite defects and/or Frenkel pairs, in-

cluding changes in the system volume, potential energy and structural parameters such the mean-square and relative mean-square atomic displacements and mean-square dispersion in the nearest-neighbor distance; (ii) defect-induced changes in the atomic structure as characterized by atomic projections, pair-correlation functions, structure factors and single-crystal diffraction patterns; and (iii) the effects of atomic structural changes on mechanical properties, particularly the irradiation dose dependence of the shear elastic constants. The amorphizability of several classes of intermetallic compounds via the introduction of antisite defects or Frenkel pairs has been systematically studied for the Cu–Ti system [20,31–33], the Ni–Zr system [19,34–37] and the B2 compounds FeTi [22,37] and NiTi [38].

Typical examples of computed defect-induced changes in physical properties, atomic structure, pair correlation function and single crystal electron diffraction pattern of the compound CuTi are shown in Fig. 2 for antisite defects and Frenkel pairs. The simulation results showed that CuTi can be amorphized by Frenkel pairs, but not by antisite defects alone [31,32]. For the case of Frenkel pairs, the onset of amorphization of CuTi is evidenced by the appearance of weak diffuse intensity halos in the calculated electron diffraction patterns at a critical dose where the potential energy per atom, $\Delta E/N$, of the disordered compound becomes approximately equal to that of the quenched liquid. In accordance with the generalized Lindemann melting criterion, this thermodynamic requirement for amorphization is satisfied at the dose where the average shear modulus of the disordered compound becomes equal to that of the amorphous phase. Furthermore, in agreement with experimental observations on ion-irradiated Zr_3Al [2,3,6], the average shear modulus of the crystalline compound decreases by about 50% prior to the onset of amorphization.

Another verification of the generalized Lindemann melting criterion via MD simulations of defect-induced

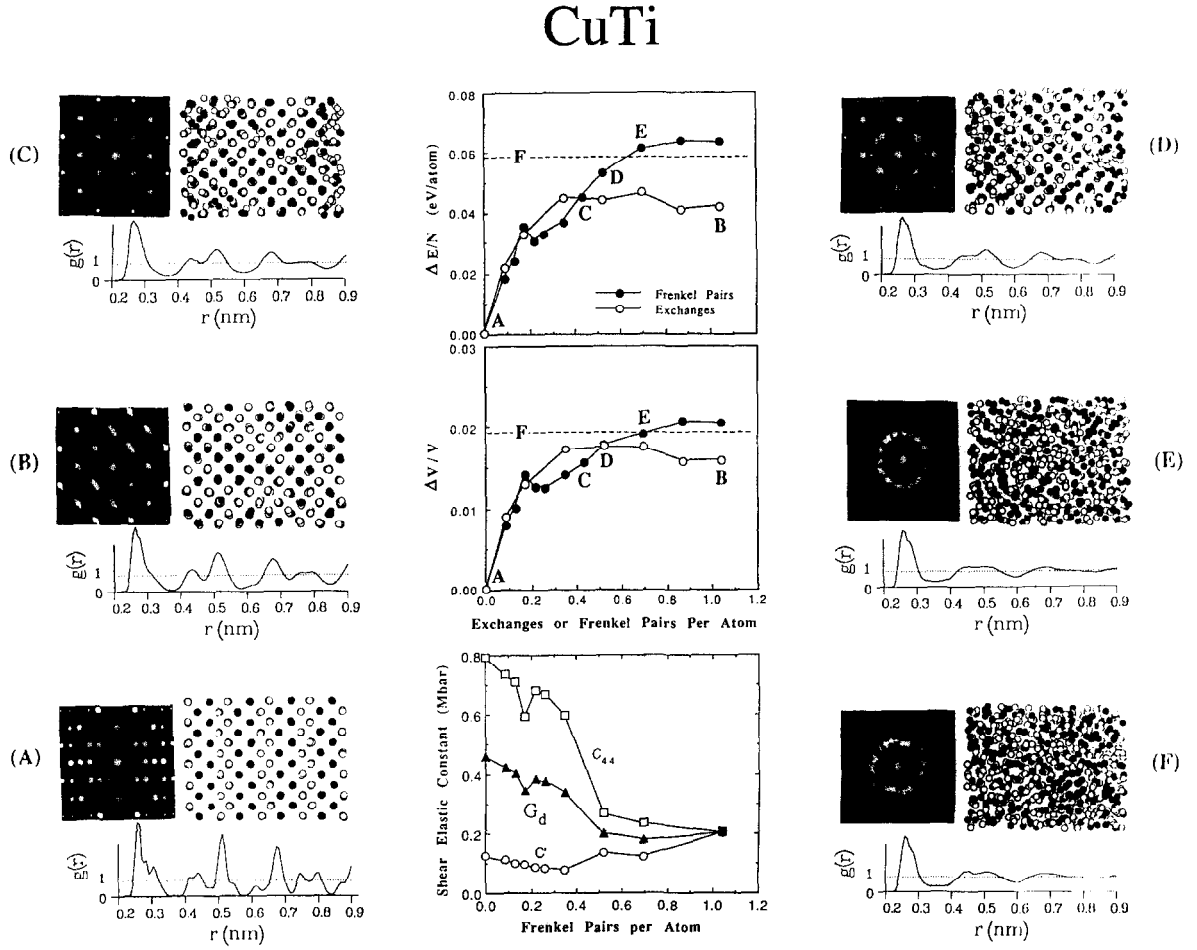

Fig. 2. Changes in the potential energy ($\Delta E/N$), volume ($\Delta V/V$) and shear elastic constants (C_{44}, C' and G_d) of CuTi as a result of increasing number of atom exchanges or Frenkel pairs per atom and evolution of the compound microstructure as characterized by progressive changes in pair-correlation function $g(r)$, [100] diffraction pattern and projection of atom positions onto the (100) plane [31,32].

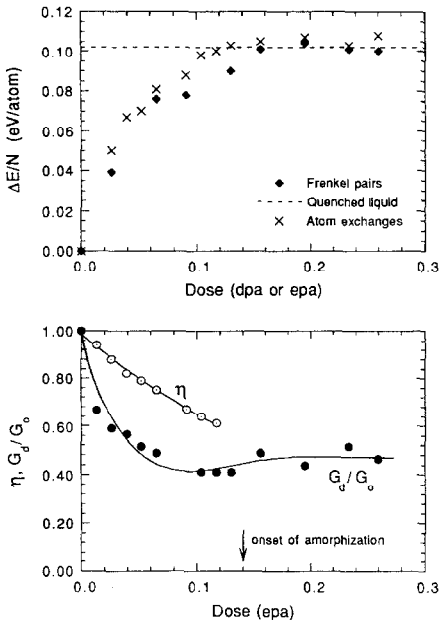

Fig. 3. Changes in the potential energy, $\Delta E/N$, long-range order parameter, η and average shear modulus, G_d, of $NiZr_2$ as a result of increasing number of atom exchanges or Frenkel pairs per atom (epa or dpa) [19]. The average shear modulus, G_d, has been normalized to the value obtained of the perfect crystal, $G_0 = 0.39$ Mbar.

amorphization is shown in Fig. 3 for the intermetallic compound $NiZr_2$. In contrast to CuTi, $NiZr_2$ can be amorphized by either Frenkel pairs or antisite defects [19]. In addition to changes in $\Delta E/N$ and G_d, the variation in the long-range order parameter η is shown. The calculated dose dependence of G_d is strikingly similar, in both qualitative and quantitative details, to the observed dose dependence of G_d in ion-irradiated Zr_3Al [2].

The values of G_d calculated for the $NiZr_2$ and FeTi compounds [19,37] are plotted in Fig. 4 as a function of change in the relative mean-square dispersion in the nearest-neighbor distance, $\delta_d^2 = (\langle \Delta R_d^2 \rangle / \langle R_d^2 \rangle - \langle \Delta R_0^2 \rangle / \langle R_0^2 \rangle)$. Here, $\langle R_d \rangle$ and $\langle R_0 \rangle$ are the mean nearest-neighbor distances in the damaged (or heated) and reference (defect-free) crystals, respectively, and the mean-square dispersion in the nearest-neighbor distance, $\langle \Delta R^2 \rangle$, is calculated by

$$\langle \Delta R^2 \rangle = \frac{1}{N} \sum_i^N \left(\langle R^2(i) \rangle - \langle R(i) \rangle^2 \right), \tag{8}$$

where N is the total number of atoms in the system and $\langle R(i) \rangle$ is the mean distance between atom i and its nearest neighbors, defined as

$$\langle R(i) \rangle = \frac{1}{M_i} \sum_j^{M_i} r_{nn}(j), \tag{9}$$

with M_i being the number of all nearest neighbors of atom i and $r_{nn}(j)$ the distance from atom i to its nearest neighbor j. The calculations of δ_d^2 were carried out using the molecular dynamics output generated previously [19,37]; however, the present calculational procedure, via Eqs. (8) and (9), was slightly different from that used in these references. In the present work, the averaged quantities, e.g. $\langle R(i) \rangle$, were updated frequently during the averaging run in order to reduce errors due to possible drifting of the mean atom positions in long simulations. For a direct comparison of the shear softening effect for the two different compounds, the values of G_d are normalized to those of the corresponding perfect crystals, G_0 (0.39 and 0.62 Mbar for $NiZr_2$ and FeTi, respectively). The data points obtained for isothermal disorder and isobaric heating lie within a narrow band, which indicates the universal nature of the dependence of G_d on δ_d^2 and, hence, on $\langle \mu_{tot}^2 \rangle$ since δ_d^2 is proportional to $\langle \mu_{vib}^2 \rangle$, as shown in Fig. 5 for the case of isobaric heating. The linear dependence is consistent with Eqs. (5) and (6), and the finding that isothermal amorphization and isobaric melting occur whenever δ_d^2 reaches a critical value provides a direct confirmation of the generalized Lindemann melting criterion.

The dependence of the Debye temperature θ_d, determined from the average shear modulus G_d, on damage dose (dpa or epa) is shown in Fig. 6 for NiZr and $NiZr_2$ [22,37]. θ_d decreases rapidly from the perfect-crystal θ_0 with increasing dose and becomes equal to the value of the

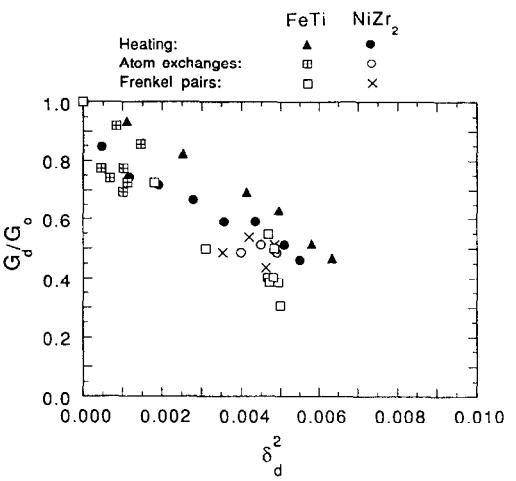

Fig. 4. Dependence of the average shear modulus, G_d, on the change in the relative mean-square dispersion in the nearest-neighbor distance, δ_d^2, calculated for the compounds $NiZr_2$ and FeTi. The average shear moduli G_d [19,37] have been normalized to the values calculated for the corresponding perfect crystals G_0 (0.62 Mbar for FeTi and 0.39 Mbar for $NiZr_2$). The simulations were carried out at 160 K (FeTi) and 30 K ($NiZr_2$). The respective values of 2.7488 Å and 3.9536×10^{-2} Å^2 and of 2.9716 Å and 9.1363×10^{-2} Å^2 were taken for $\langle R_0 \rangle$ and $\langle \Delta R_0^2 \rangle$.

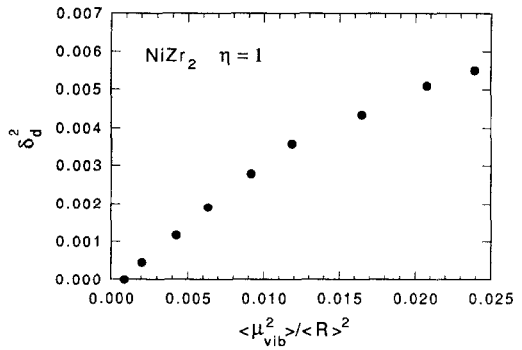

Fig. 5. Relationship between the change in the relative mean-square dispersion in the nearest-neighbor distance, δ_d^2 and the mean-square dynamic atomic displacement, $\langle \mu_{vib}^2 \rangle / \langle R \rangle^2$ during isobaric heating of $NiZr_2$.

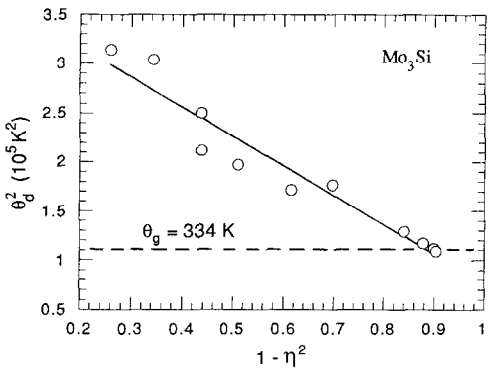

Fig. 7. Linear relationship between θ_d^2 and $(1-\eta^2)$ measured on neutron-irradiated Mo_3Si [44].

glassy phase at the onset of amorphization. The calculated values of θ_0 and θ_g were ~ 315 and 200 K for NiZr, and 260 and 180 K for $NiZr_2$, respectively, in agreement with experimental measurements on the two compounds [39–41].

3.2. Experimental observations

One of the strongest experimental supports of the generalized Lindemann melting criterion is provided by Brillouin scattering study on ion-bombarded Zr_3Al [2,3] which showed that, during irradiation, the onset of amorphization occurred when the average sound velocity in the defective compound became equal to that in the amorphous phase.

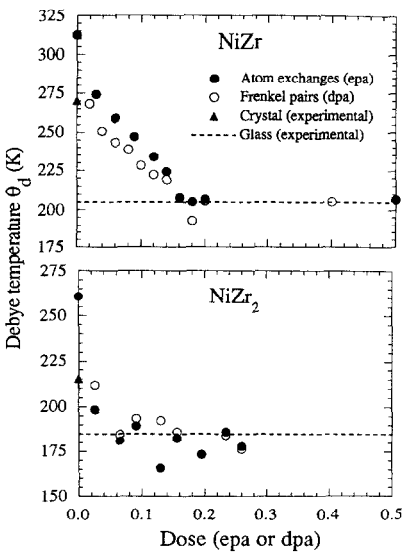

Fig. 6. Damage-dose dependence of the Debye temperature θ_d calculated for NiZr and $NiZr_2$ [37]. The experimental values for the undamaged crystalline compounds [39,40] and glassy alloys [41] are indicated.

Since the average sound velocity is proportional to the square root of the average shear modulus, G_d [24], this equality confirms the validity of Eq. (7) which predicts that the enthalpy difference between the amorphous phase and the defective crystal vanishes when their average shear moduli, as measured by Debye temperatures, become equal. Furthermore, the square of the average sound velocity in the defective crystalline compound was a linearly decreasing function of $(1-\eta^2)$ and, hence, of $\langle \mu_{sta}^2 \rangle$ [26,42,43], in agreement with Eq. (5), and became insensitive to further disorder when η reached a critical value at the onset of amorphization. The same behavior was also observed on neutron-irradiated Mo_3Si [44], as shown in Fig. 7. The squared Debye temperature of the damaged compound, θ_d^2, was found to decrease linearly with increasing $(1-\eta^2)$. Above a critical state of disorder, corresponding to $\eta \approx 0.3$ where θ_d became equal to θ_g, the compound became amorphous.

The prediction that amorphization is triggered whenever the mean-square static displacement attains a critical value is confirmed by the results of ion-implantation studies [45–49]. An example is shown in Fig. 8 for the case of B implantation into Nb [45]. Here, the structural changes in the implanted matrix were monitored using X-ray diffraction: the average static atomic displacement μ_{sta} of the lattice atoms was derived from a static Debye–Waller factor given by the slope of a modified Wilson plot and the volume fraction of the amorphous phase determined from the intercept of this plot with the X-ray intensity axis. It was found that μ_{sta} increased rapidly with increasing implantation dose and approached a saturation level for B concentrations above ~ 5 at.%. When μ_{sta} attained a maximum, critical value of ~ 0.14 Å, amorphization began, and the fraction of the amorphous material in the implanted sample increased rapidly to 100%. Similar features were found for Mn implantation-induced amorphization of Al [48,49].

Sufficient hydrogenation can also lead to amorphization of binary intermetallic compounds in which one alloy

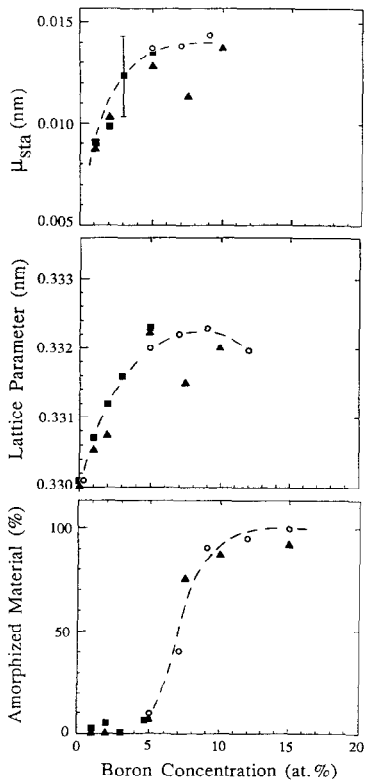

Fig. 8. Plots of the average static atomic displacement μ_{sta}, lattice parameter, and volume fraction of the amorphized material versus the concentration of B atoms implanted into Nb [45].

component has a large negative enthalpy of mixing with hydrogen (see Ref. [50] and references therein). Recent in situ high-voltage electron-microscopy investigations showed that pre-doping of one of these compounds, Zr_3Al [51], with small amounts of hydrogen caused a twenty-fold reduction in the electron dose necessary to amorphize the compound. Indeed, hydrogen pre-doping introduces additional static displacements which reduce the contribution from radiation-generated defects necessary to induce the amorphizing transformation.

According to our thermodynamic criterion for amorphization, Eq. (7), a compound that has a smaller difference in the Debye temperatures between its crystalline and amorphous states, $(\theta_0 - \theta_g)$, is more susceptible to defect-induced amorphization than a compound that has a larger difference. This prediction is supported by recent measurements. For example, the critical doses for amorphization of the compounds $NiZr_2$, NiZr and Ni_3Zr by electron irradiation below 30 K were found to be 0.22, 0.37 and 3.18 dpa, respectively [52]. The Debye temperatures were also measured for these ordered compounds [39,40] and several amorphous alloys [41] of the Ni–Zr system. Indeed, the difference between the Debye temperatures of the crystalline and amorphous states is smallest for $NiZr_2$, intermediate for NiZr and largest for Ni_3Zr.

With $\langle \mu_{sta}^2 \rangle$ being a measure of the solute concentration, the plot of T_m^d versus $\langle \mu_{sta}^2 \rangle$, Fig. 1b, represents a generalization of the rapidly-plunging, constant-composition T_0-curves describing polymorphous melting of terminal solid solutions of binary phase diagrams. The T_0-curve should reflect the compositional dependence of the Debye temperature of the crystalline state, θ_d. Since the intersection of the θ_d-plot and the θ_g-line defines a critical value of the mean-square static displacement, $\langle \mu_m^2 \rangle$, beyond which the defective crystal becomes thermodynamically unstable relative to the glass, the minimum solute concentration required for glass formation is also defined by the intersection of the T_0-curve of terminal solid solution with the relatively flat T_g-curve determined for amorphous phases. This prediction has been verified for many binary alloy systems [53].

The glass transition temperature T_g has been determined for a number of compounds in recent experiments on radiation-induced amorphization. Measurements on CuTi, for example, are shown in Fig. 9 [54]. T_g is found to be ~ 575 K, which is comparable with the temperature at which equilibrium short-range order is achieved during isochronal annealing of irradiated and unirradiated amorphous $Cu_{64}Ti_{36}$ alloys [55], and is close to the ideal glass transition temperature determined by extrapolating the results of slow, continuous heating of amorphous Cu–Ti ribbons [56] to zero heating rate. The values of T_g obtained for NiAl and NiTi are 240 and 600 K, respectively [57]. Fig. 9 also shows that, for any given type of irradiating

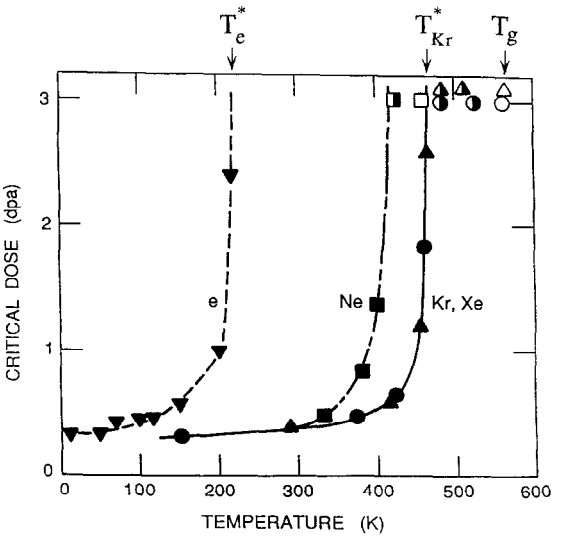

Fig. 9. Temperature dependence of the critical dose for amorphization of the compound CuTi during irradiation with electrons, Ne^+, Kr^+, and Xe^+ ions [54]. The temperatures T_g and T^* are indicated.

particles, there is a critical temperature T^* above which complete amorphization is not possible. This temperature should not be taken as T_g; it reflects various kinetic effects that cannot be accounted for by the generalized Lindemann model. For example, for electron-induced amorphization, $T_e^* \approx 220$ K is governed mainly by the defect-production rate and migration energy of the mobile defects that tend to restore long-range order; it is the temperature at which the long-range order parameter abruptly decreases from 1 to ~ 0.2 [58]. For heavy-ion irradiation with similar dose rates, T^* was found to increase with increasing ion mass, approaching the value of T_g. In this case, T^* was the temperature at which small amorphous zones created in a crystalline matrix by ion impact became unstable with respect to recrystallization via growth of the crystalline phase [54].

4. Conclusion

The present work has shown that the thermodynamics of crystalline-to-amorphous transformations can be formally described by a simple theory of melting based on a generalized version of the Lindemann melting criterion. This criterion assumes that melting of a metastable crystal occurs when the sum of the dynamic and static mean-square atomic displacements reaches a critical value identical to that for melting of the perfect crystal. It requires that the melting temperature of a defective crystal must decrease with increasing static atomic disorder and leads to a universal polymorphous melting curve for metastable crystals when the melting temperature is plotted as a function of mean-square static displacement. Within the framework of this more general melting concept, the crystalline-to-amorphous transformation is simply melting of a critically disordered crystal at temperatures where the supercooled liquid exists in a configurationally-frozen state, i.e. the glassy state. The real significance of this new conceptual approach to damage processes is that the melting criterion is independent of the physical origin of the static atomic displacement. Thus, the concept of disorder-induced melting should be applicable to local regions of the crystal such as high-angle grain boundaries or the highly-strained crack tip regions of solids where static atomic displacements are concentrated.

Acknowledgements

The present study has greatly benefitted from useful discussions and past collaboration with many colleagues, in particular R. Devanathan, M. Meshii, L.E. Rehn, and M.J. Sabochick. We are indebted to all of them. This work was supported by the US Department of Energy, Basic Energy Sciences-Materials Sciences, under contract W-31-109-Eng-38.

References

[1] W.L. Johnson, Prog. Mater. Sci. 30 (1986) 81.
[2] P.R. Okamoto, L.E. Rehn, J. Pearson, R. Bhadra, M. Grimsditch, J. Less Common Met. 140 (1988) 231.
[3] L.E. Rehn, P.R. Okamoto, J. Pearson, R. Bhadra, M. Grimsditch, Phys. Rev. Lett. 59 (1987) 2987.
[4] K.C. Russell, Prog. Mater. Sci. 28 (1985) 229.
[5] D.E. Luzzi, M. Meshii, Res. Mech. 21 (1987) 207.
[6] P.R. Okamoto, M. Meshii, in: H. Wiedersich, M. Meshii (Eds.), Science of Advanced Materials (American Society for Metals, Metals Park, OH, 1990) p. 33.
[7] A.T. Motta, J. Nucl. Mater. 244 (1997) 227.
[8] J.L. Tallon, J. Phys. Chem. Solids 41 (1984) 837.
[9] J.L. Tallon, Philos. Mag. A39 (1979) 151.
[10] M. Grimsditch, K.E. Gray, R. Bhadra, R.T. Kampwirth, L.E. Rehn, Phys. Rev. B35 (1987) 883.
[11] R.P. Sharma, R. Bhadra, L.E. Rehn, P.M. Baldo, M. Grimsditch, J. Appl. Phys. 66 (1989) 152.
[12] J. Koike, P.R. Okamoto, R.E. Rehn, R. Bhadra, M. Grimsditch, M. Meshii, Mater. Res. Soc. Symp. Proc. 157 (1990) 777.
[13] J. Zuk, H. Kiefte, M.J. Clouter, J. Appl. Phys. 73 (1993) 4851.
[14] R. Devanathan, N. Yu, K.E. Sickafus, M. Nastasi, J. Nucl. Mater. 232 (1996) 59.
[15] G. Grimvall, S. Sjödin, Phys. Scr. 10 (1974) 340.
[16] A. Voronel, S. Rabinovich, A. Kisliuk, V. Steinburg, T. Sverbilova, Phys. Rev. Lett. 60 (1988) 2402.
[17] F.A. Lindemann, Z. Phys. 11 (1910) 609.
[18] R. Devanathan, N.Q. Lam, P.R. Okamoto, M. Meshii, Mater. Res. Soc. Symp. Proc. 291 (1993) 653.
[19] R. Devanathan, N.Q. Lam, P.R. Okamoto, M. Meshii, Phys. Rev. B48 (1993) 42.
[20] N.Q. Lam, P.R. Okamoto, R. Devanathan, M. Meshii, in: P.E.A. Turchi, A. Gonis (Eds.), Statics and Dynamics of Alloy Phase Transformations, NATO ASI Series B: Physics, vol. 319 (Plenum Press, New York, 1994) p. 691.
[21] N.Q. Lam, P.R. Okamoto, Surf. Coatings Technol. 65 (1994) 7.
[22] N.Q. Lam, P.R. Okamoto, Mater. Res. Soc. Bull. XIX (7) (1994) 41.
[23] H. Kleinert, Gauge Fields in Condensed Matter, vol. II (World Scientific, Singapore, 1989).
[24] G. Grimvall, Thermophysical Properties of Materials, Selected Topics in Solid State Physics, vol. XVIII (North-Holland, Amsterdam, 1986).
[25] B.E. Warren, X-Ray Diffraction (Addison-Wesley, Reading, MA, 1969).
[26] M.A. Krivoglaz, Theory of X-Ray and Thermal-Neutron Scattering by Real Crystals (Plenum Press, New York, 1969) p. 83.
[27] E.A. Stern, K. Zhang, Phys. Rev. Lett. 60 (1988) 1872.
[28] H.A. Atwater, W.L. Brown, Appl. Phys. Lett. 56 (1990) 30.
[29] J.A. Eastman, M.R. Fitzsimmons, J. Appl. Phys. 77 (1995) 522.
[30] P.R. Okamoto, J. Heuer, N.Q. Lam, S. Ohnuki, Y. Matsukawa, K. Tozawa, submitted for presentation in: Symp. B: Phase Transformations and Systems Driven far from Equilibrium, MRS Meeting, Boston, 1997, to be published.
[31] M.J. Sabochick, N.Q. Lam, Phys. Rev. B 43 (1991) 5243.

[32] N.Q. Lam, P.R. Okamoto, M.J. Sabochick, R. Devanathan, J. Alloys Compounds 194 (1993) 429.
[33] D.T. Kulp, T. Egami, D.E. Luzzi, V. Vitek, J. Alloys Compounds 194 (1993) 417.
[34] C. Massobrio, V. Pontikis, G. Martin, Phys. Rev. B41 (1990) 10486.
[35] C. Massobrio, V. Pontikis, Phys. Rev. B45 (1992) 2484.
[36] R. Devanathan, N.Q. Lam, M.J. Sabochick, P.R. Okamoto, M. Meshii, J. Alloys Compounds 194 (1993) 447.
[37] R. Devanathan, PhD thesis, Northwestern University, 1993.
[38] M.J. Sabochick, N.Q. Lam, Mater. Res. Soc. Symp. Proc. 201 (1991) 387.
[39] R. Kuentzler, J. Phys. F14 (1984) L79.
[40] A. Amamou, R. Kuentzler, Y. Dossmann, P. Forey, J.L. Glimois, J.L. Feron, J. Phys. F12 (1982) 2509.
[41] D.G. Onn, L.Q. Wang, Y. Obi, K. Fukamichi, Solid State Commun. 46 (1983) 37.
[42] R.D. Burbank, R.C. Dynes, J.M. Poate, J. Low Temp. Phys. 36 (1979) 573.
[43] E.V. Kozlov, V.M. Dementryev, V.N. Emelyanov, N.M. Kormin, A.S. Taylashev, D.M. Stern, in: H. Warlimont (Ed.), Order–Disorder Transformation in Alloys (Springer-Verlag, Berlin, 1974) p. 58.
[44] A.V. Mermel'shteyn, A.Ye. Kar'kin, V.Ye. Arkhipov, V.I. Voronin, Phys. Met. Metall. 55 (1983) 67.
[45] G. Linker, Mater. Sci. Eng. 69 (1985) 105.
[46] G. Linker, Solid State Commun. 57 (1986) 773.
[47] G. Linker, Nucl. Instrum. Meth. B 19&20 (1987) 526.
[48] A. Seidel, S. Massing, B. Strehlau, G. Linker, Phys. Rev. B38 (1988) 2273.
[49] A. Seidel, G. Linker, O. Meyer, J. Less-Common Met. 145 (1988) 89.
[50] W.J. Meng, P.R. Okamoto, L.E. Rehn, in: H. Wiedersich, M. Meshii (Eds.), Science of Advanced Materials (American Society for Metals, Metals Park, OH, 1990) p. 99.
[51] W.J. Meng, J. Koike, P.R. Okamoto, L.E. Rehn, Mater. Res. Soc. Symp. Proc. 128 (1989) 345.
[52] G. Xu, M. Meshii, P.R. Okamoto, L.E. Rehn, J. Alloys Compounds 194 (1993) 401.
[53] P.R. Okamoto, N.Q. Lam, L.E. Rehn, to be published.
[54] J. Koike, P.R. Okamoto, R.E. Rehn, M. Meshii, J. Mater. Res. 4 (1989) 1143.
[55] G. Schumacher, S. Klaumünzer, W. Petry, U. Dedek, J. Phys. F18 (1988) 1681.
[56] T.B. Massalski, C.G. Woychik, Acta Metall. 33 (1985) 1873.
[57] P. Moine, C. Jaouen, J. Alloys Compounds 194 (1993) 373.
[58] G. Xu, PhD thesis, Northwestern University, 1993.